ResearchGate

See discussions, stats, and author profiles for this publication at: https://www.researchgate.net/publication/282680030

A Thermoreversible Supramolecular Polyurethane with Excellent Healing Ability at 45 °C

ARTICLE *in* MACROMOLECULES · SEPTEMBER 2015

Impact Factor: 5.8 · DOI: 10.1021/acs.macromol.5b01162

READS

34

9 AUTHORS, INCLUDING:

C. Paul Buckley

University of Oxford

119 PUBLICATIONS **1,462** CITATIONS

SEE PROFILE

Ian W Hamley

University of Reading

404 PUBLICATIONS **11,802** CITATIONS

SEE PROFILE

Available from: Ian W Hamley
Retrieved on: 27 January 2016

Macromolecules

Article

pubs.acs.org/Macromolecules

A Thermoreversible Supramolecular Polyurethane with Excellent Healing Ability at 45 °C

Antonio Feula,[†] Alexander Pethybridge,[†] Ioannis Giannakopoulos,[‡] Xuegang Tang,[‡] Ann Chippindale,[†] Clive R. Siviour,[‡] C. Paul Buckley,[‡] Ian W. Hamley,[†] and Wayne Hayes*[,†]

[†]Department of Chemistry, University of Reading, Whiteknights, Reading RG6 6AD, U.K.

[‡]Department of Engineering Science, Oxford University, Parks Road, Oxford OX1 3PJ, U.K.

Supporting Information

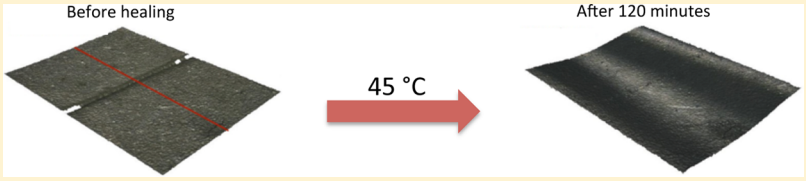

ABSTRACT: We report the synthesis and characterization of a healable, elastomeric shape recovery supramolecular polyurethane whose properties result from self-complementary $\pi-\pi$ stacking and hydrogen bonding interactions plus phase separation. ESEM analysis and photographic images have revealed that this material can heal at 45 °C in 15 min to recover the mechanical properties of the pristine material with healing efficiencies >99%. This supramolecular polyurethane is also able to recover an applied strain of 25% within 5 min of release of the load.

Downloaded by UNIV OF READING on September 8, 2015 | http://pubs.acs.org
Publication Date (Web): August 21, 2015 | doi: 10.1021/acs.macromol.5b01162

INTRODUCTION

Polyurethanes are an important class of polymers that have been used in a wide range of applications.[1−5] They can be synthesized easily by addition of diols or polyols to polyisocyanates.[6,7] Furthermore, the introduction of chain extenders and carefully selected end-groups has played a crucial role in the tunability of their mechanical properties.[8−12]

Recently, several groups have reported[2,13,14] the development of low molecular weight polyurethanes that feature end-groups which can assemble via combinations of hydrogen bonding and $\pi-\pi$ stacking interactions to afford supramolecular networks possessing physical properties comparable to high molecular weight counterparts. These so-called "supramolecular polyurethanes" possess thermoreversible characteristics as result of the weak noncovalent interactions within their networks.[15,16]

The development of healable polymers which are capable of repairing damage to surfaces or within the bulk material is an extremely attractive proposition within many industrial applications.[17−19] To this end, materials able to heal in an autonomous fashion[20−22] or via application of external stimuli such as heat,[23−25] light,[26−28] or pressure have been generated.[29,30] Several approaches to healable materials have been described including irreversible covalent bond formation,[31,32] utilization of reversible covalent bonds,[33−37] release of encapsulated liquid monomers,[20,38−40] or the employment of weak noncovalent interactions such as aromatic $\pi-\pi$ stacking,[41−46] hydrogen bonds,[22,23,30,41,47−59] or metal−ligand bonds.[60−62]

We have reported the development of a highly efficient healable supramolecular network based upon a two-component blend.[41,63] Within this research program, Burattini et al. reported an elastomeric healable supramolecular polymer network formed by $\pi-\pi$ stacking interactions between a telechelic polyurethane equipped with pyrenyl end-groups and a chain-folding polydiimide receptor.[41] The blend was cut, and the mechanical properties of the material were recovered after exposure to an elevated temperature (100 °C) for a period of 240 min. The tensile modulus, elongation to break, and modulus of toughness recovered to 95, 91, and 77% of their original values, respectively. As a control experiment, a cut specimen of the pyrenyl end-capped polyurethane was also exposed to the same healing regime. In contrast to the blend, the rheological characteristics of the polyurethane remained elastic up to 100 °C and the cut did not heal, indicating that dissociation of the $\pi-\pi$ stacking interactions was a crucial design element responsible for the healing characteristics of the two-component blend.

In this paper we describe the synthesis and studies of a supramolecular polyurethane network whose mechanical properties can be recovered in 15 min, after a film is cut and healed by exposure to an elevated temperature of only 45 °C. This polyurethane is self-complementary: just one component is needed to achieve the required interactions, in contrast to above-mentioned studies on complementary supramolecular polymer blends.[25] The polyurethane was designed to permit a combination of hydrogen bonding and aromatic $\pi-\pi$ stacking interactions plus phase separation in the bulk to facilitate

Received: May 29, 2015
Revised: July 30, 2015
Published: August 21, 2015

© 2015 American Chemical Society

DOI: 10.1021/acs.macromol.5b01162
Macromolecules 2015, 48, 6132−6141

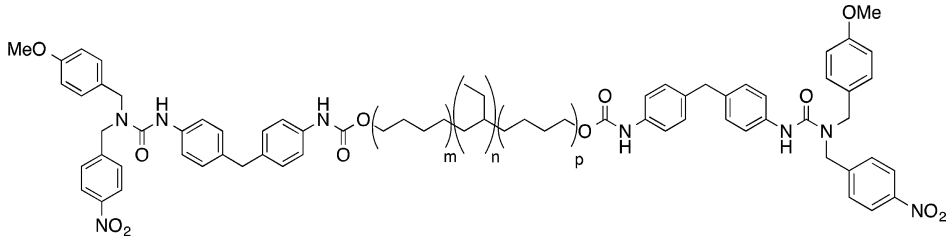

Figure 1. Structure of polyurethane **1**.

Scheme 1. Synthesis of 1-(4-Methoxybenzyl)-1-(4-nitrobenzyl)-3-phenylurea 2

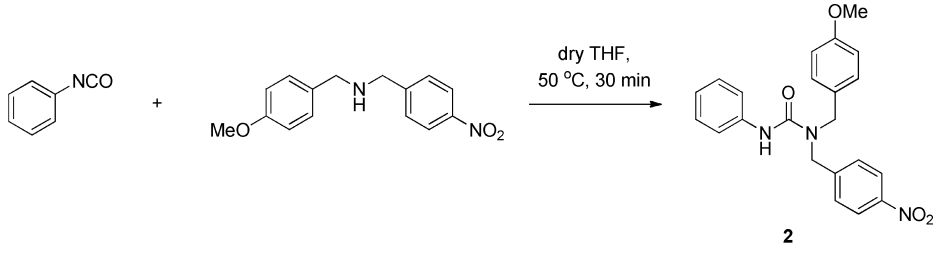

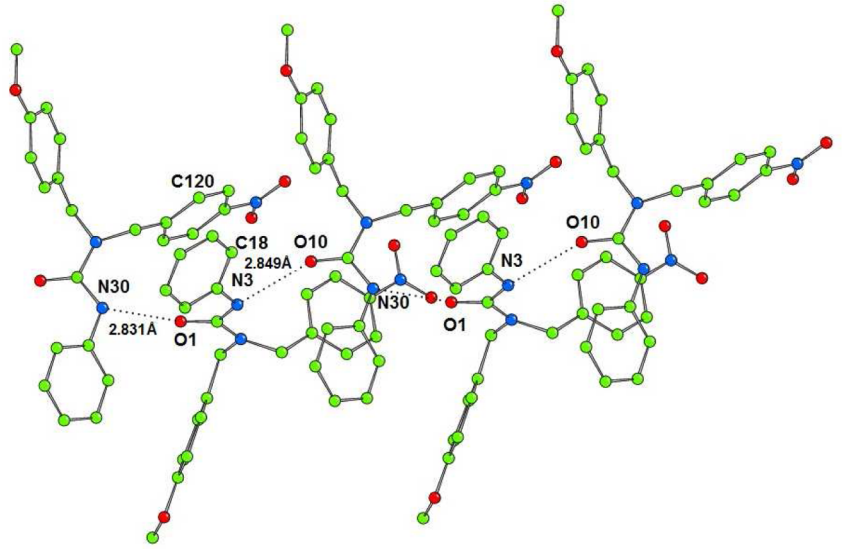

Figure 2. Solid state structure of the urea **2** revealing hydrogen bonding and $\pi-\pi$ stacking interactions between the urea and phenyl groups, respectively. The hydrogen atoms have been omitted for clarity, and the dashed lines correspond to the N(30)···O(1) and N(3)···O(10) distances involved in hydrogen bonding.

Downloaded by UNIV OF READING on September 8, 2015 | http://pubs.acs.org
Publication Date (Web): August 21, 2015 | doi: 10.1021/acs.macromol.5b01162

network assembly. As a consequence of the molecular design of this polyurethane, we have achieved an elastomeric material that can be healed at readily accessed temperatures, and it thus offers promise in surface coatings, adhesive formulations, or complex multicomponent assemblies that will not withstand exposure to more intensive thermal treatment.

RESULTS AND DISCUSSION

The aim of this study was to install an end-group onto a polyurethane capable of self-assembling via the combination of hydrogen bonding and aromatic $\pi-\pi$ stacking interactions in order to develop a healable polymer with tunable physical and mechanical properties. *N*-(4-Methoxybenzyl)-1-(4-nitrophenyl)methanamine was synthesized[64,65] via a two-step process (see Supporting Information Figures S1 and S2) and used as the polymer end-group. Using an established synthetic protocol,[8,9,41] Krasol HLBH-P2000 was first reacted with methylene diphenyl diisocyanate (MDI) at 80 °C to form a prepolymer featuring isocyanate end-groups. Subsequent addition of *N*-(4-methoxybenzyl)-1-(4-nitrophenyl)-methanamine to the prepolymer afforded the desired polyurethane **1** in a yield of 88% (see Figure 1 plus Figures S3 and S4).[9] IR spectroscopic analysis confirmed the disappearance of the characteristic isocyanate stretch at 2340 cm^{-1}, and ^1H NMR spectroscopy revealed the appearance of the key methylene protons resonance adjacent to the newly formed urea group. Variable temperature FT-IR was also performed, and a shift of the urethane carbonyl absorption band from 1708 cm^{-1} at 30 °C to 1727 cm^{-1} at 60 °C was observed, indicating that dissociation of the hydrogen-bonding interactions occurs at 60 °C (see Figures S5 and S6). These spectroscopic data are consistent with literature concerning the assembly of polyurethanes.[15,66]

Chain extension was minimal; as ascertained by ^1H NMR spectroscopic analysis, the ratio of the integrals of the proton resonances of the urethane groups of the polymer relative to

DOI: 10.1021/acs.macromol.5b01162
Macromolecules 2015, 48, 6132−6141

those of the urea groups of the end-capping units was 1:1. Gel permeation chromatography (GPC) analyses of the prepolymer Krasol HLBH-P2000 and polyurethane **1** were also compared, and the values were M_n = 3795 and M_n = 6056, respectively. Differential scanning calorimetry (DSC) of the resultant polyurethane revealed a glass transition (T_g) at ca. −43 °C (Figure S7), indicating that installation of the polar end-groups had not dramatically affected the flexibility of the apolar polyethylene-*co*-butylene central block (T_g −46 °C). Both Krasol HLBH-P2000 and the diisocyanate prepolymer are thick viscous liquids at room temperature whereas, in contrast, polyurethane **1** is a solid material indicating the crucial role of the end-groups in the assembly of supramolecular networks.

In order to understand the role of the end-groups in the formation of the supramolecular polymer network, *N*-(4-methoxybenzyl)-1-(4-nitrophenyl)methanamine was reacted with phenyl isocyanate to obtain 1-(4-methoxybenzyl)-1-(4-nitrobenzyl)-3-phenylurea **2** in 92% yield (Scheme 1; see Figures S8 and S9).

X-ray crystallographic analysis of the urea **2** revealed key hydrogen bonds between the urea groups in adjacent molecules (N(3)···O(10), 2.849(5), and N(30)···O(1), 2.831(5)Å) (Figure 2, Table S1, Figure S10). In addition, there are weak $\pi-\pi$ stacking interactions between the phenyl rings containing C(18) and C(120) (the distance between the centroid of the phenyl ring containing C(120) to the plane containing C(18) is 3.081 Å) (see Figure S11).

In order to understand the morphology of polyurethane **1**, wide-angle X-ray scattering (WAXS) and small-angle X-ray scattering (SAXS) were both investigated under variable temperature regimes (30−70 °C). The WAXS scattering pattern shows a lattice spacing of 5.64 Å, corresponding to the stacking of the urea moieties (Figure 3).[67] It is interesting

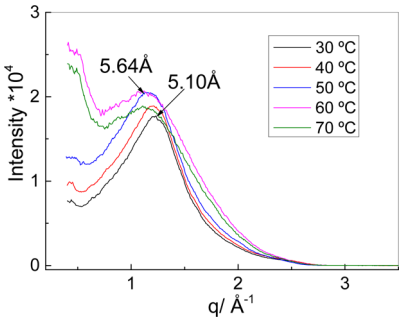

Figure 3. Variable temperature WAXS of polyurethane **1**.

to note that with the temperature increasing the lattice spacing becomes consistently less sharp, suggesting that the hydrogen bonding interactions between the urea moieties are being disrupted. In particular, a change of the morphology that starts at the temperature of 60 °C was observed in agreement with rheological data also acquired (*vide infra*).

A single Bragg peak (55 Å) was evident in the SAXS data (Figure 4), suggesting a microseparated morphology, which is the result of the immiscibility of the hard hydrogen bonding end-groups with the soft polymer backbone. In addition, a drastic change in the morphology was visible at the temperature of 60 °C in the SAXS profile indicating that the supramolecular network was being disrupted.

The rheological behavior of a film of polyurethane **1** solution cast from THF was then characterized—a summary of the data

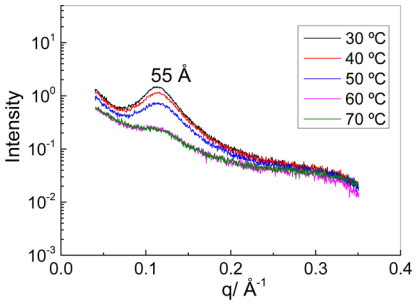

Figure 4. Variable temperature SAXS of polyurethane **1**.

obtained is shown in Figure 5. At low temperatures (ca. 10 °C), the shear storage modulus (G') and loss modulus (G'') decrease gradually with increasing temperature. However, the decrease in G' accelerates above 40 °C, owing to the dissociation of the supramolecular polyurethane network, resulting in a large degree of softening. It is also observed that the storage modulus and loss modulus cross at a temperature of 55 °C, indicating a nominal transition from an elastic behavior to a viscous state. The master curve in Figure 5b was constructed by manual shifting of isothermal frequency sweep data obtained at frequencies between 0.1 and 100 rad s^{-1} and at 5 °C intervals between −30 and −10 and 10 °C intervals between −10 and +80 °C (Figure S12).[68] The master curve shows a typical terminal zone, transition zone to flow, plateau zone (rubbery), and transition zone to glassy behavior, as indicated in Figure 5b. The terminal zone reveals weak entangled polymer melt behavior for polyurethane **1**. Polyurethane **1** was also subjected to repeated frequency sweeps on a single specimen over the course of three temperature cycles, and the data obtained indicated that the properties did not change significantly between cycles (Figure S13).

Figure 6a shows the shift factors, a_T, used to produce the master curves, as a function of temperature. It is observed that a_T changes by some 10 orders of magnitude between −30 and +80 °C and that the graph is split into two approximately linear zones (indicated as zone 1 and zone 2) with a transition between these regions. The data indicate that two processes may be involved in determining the temperature dependence of the mechanical response. Furthermore, the large change in a_T over a small, readily accessible temperature range is consistent with the dissociation of the supramolecular network, which leads to a large drop in viscosity and indicates that this material does not behave like a conventional thermoplastic.[25,41,69]

Figure 6b shows a shift factor plot for the polyurethane **1** as a function of temperature normalized with respect to T_g. The behavior is consistent with other supramolecular polymer systems[41,70]—two linear zones are evident, with a transition associated with the dissociation of the network. Polyurethane **1** thus does not exhibit thermoplastic characteristics traditionally associated with high molecular weight polymers, which normally show just one linear zone without the additional transition. The gradient of the curve at high temperatures is significantly larger than that observed at low temperatures. In the case of amorphous, covalently bonded polymers, a linear relationship exists between a_T and normalized temperature;[71,72] however, this relationship has been observed to break down for supramolecular polymers.[25,41,69] This dramatic change was attributed to additional relaxation processes, which do not occur in amorphous covalently bonded polymers and to the

Downloaded by UNIV OF READING on September 8, 2015 | http://pubs.acs.org
Publication Date (Web): August 21, 2015 | doi: 10.1021/acs.macromol.5b01162

DOI: 10.1021/acs.macromol.5b01162
Macromolecules 2015, 48, 6132−6141

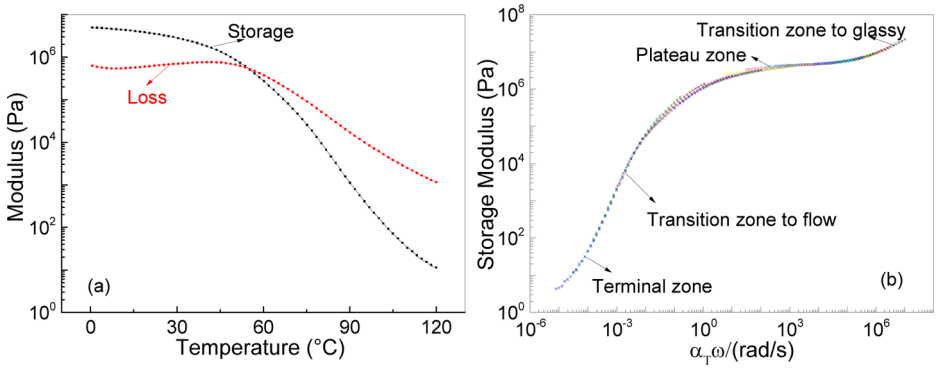

Figure 5. Variation of complex shear modulus with temperature and frequency for polyurethane **1**: (a) temperature sweep at 5 Hz; (b) master curve at a reference temperature of 30 °C. Colors indicate different temperatures, and more detailed data are available in the Supporting Information (Figures S12 and S13).

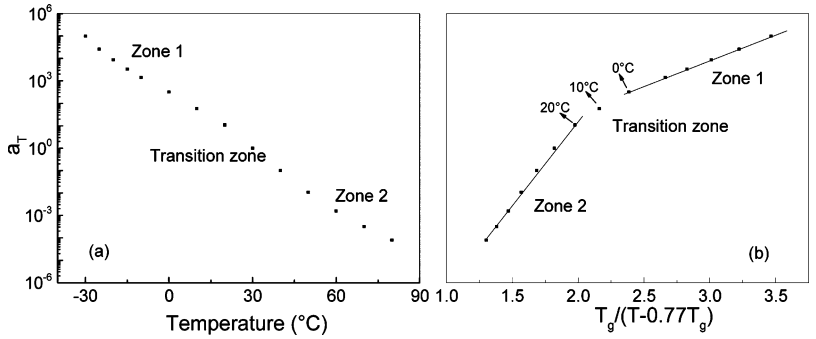

Figure 6. (a) Time–temperature shift factor a_T of polyurethane **1** as a function of temperature. (b) Plot of a_T for polyurethane **1** as a function of temperature normalized to T_g.

disengagement of the supramolecular ($\pi-\pi$ stacking and hydrogen bonding) interactions.[41,70] Overall, therefore the mechanical response of polyurethane **1** is comparable to other reported supramolecular polymers, but the temperature at which the noncovalent interactions break down is markedly lower.[23,50]

To investigate the healing potential of the material, the mechanical responses of strips of the film (ca. 0.5 mm thick, 40 mm long, and 5 mm wide) were analyzed in both the "pristine" and "healed" material. The healed samples were produced as follows. First, a sample of the above dimensions was cut in the center gently, transverse to its long axis with a razor, and then positioned with the cut edges in close proximity (not overlapped or pressed into contact with each other as in related studies),[32,63,73,74] which was placed on a flat glass substrate, not in a mold. The samples were then placed in an oven and held at 45 °C for 120 min. This temperature was selected based on analysis of the characterization data above: clear changes in the morphology are observed at temperatures of 60 °C and above, and these are accompanied by a significant reduction in the storage modulus. This places an upper limit on the temperature at which we can expect healing to take place while retaining the overall shape of the material. Furthermore, the transition zone in Figure 6b occurs at temperatures up to ca. 20 °C. In previous studies, this transition has been associated with healing ability in polymers, and it is certainly associated with changes in the structure of the material. After preliminary tests in which the healing process was visually monitored, 45 °C was selected as the healing temperature. This temperature was found to give a good combination of healing time and ability to retain the overall specimen structure. It is of course expected that healing would occur (more slowly) at lower temperatures. At higher temperatures, healing is evident, but the sample suffers from creep, especially above ca. 55 °C, as expected from the rapid drop in storage modulus above 60 °C. The pristine samples were also subjected to the same heat treatment, but without the initial cut.

The dynamics of the healing process were observed in three ways. In all cases, a Peltier heating system was used to maintain the temperature at 45 °C during the healing process. To observe the healing on the macroscale, the process was monitored with an optical camera. On the microscale another specimen was monitored in an environmental scanning electron microscope (ESEM). Micrographs from both experiments are shown in Figure 7, with additional images provided in the Figures S14 and S15. Figure 7A,a shows a neat cut across the whole sample with the generation of ridges in some areas. The images in Figure 7B,b also show the material after 2 h healing at 45 °C. While there is some evidence of the crack location, the crack has healed and the area surrounding it has the same roughness profile as the rest of the specimen.

The healing process was further quantified using an optical surface profilometer to produce 3D depth information, as shown in Figure 8; the precision of the measurements was approximately 0.01 μm. The first profile, taken prior to healing, reveals the cut at the center of the specimen. A line profile, taken down the length of the specimen as indicated, shows a peak and trough at the crack location. However, during the healing process, the cut quickly closes, and after approximately 30 min the profile at the gap location is already similar elsewhere in the specimen, although the presence of the cut is still visible in the reconstructed surface profile. After 120 min,

Downloaded by UNIV OF READING on September 8, 2015 | http://pubs.acs.org
Publication Date (Web): August 21, 2015 | doi: 10.1021/acs.macromol.5b01162

DOI: 10.1021/acs.macromol.5b01162
Macromolecules 2015, 48, 6132–6141

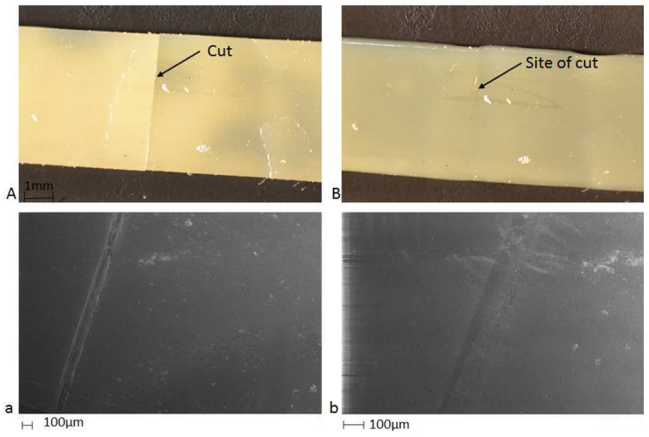

Figure 7. Observation of the healing of polyurethane 1 at 45 °C before (A, a) and after 2 h (B, b) at the macroscale by camera (A, B) and microscale by ESEM analysis (a, b). Additional images of the healing process can be found in Figures S14 and S15.

the roughness around the cut area is both qualitatively (i.e., visibly) and quantitatively comparable to the other areas in the surface of the sample, indicating a fully topographical recovery of the cut interface. It should be noted that in this analysis the vertical scale is greatly enlarged with respect to the horizontal: the gradients in the surface roughness are not enough to drive surface smoothing on the time scale of the experiment.

The above data reveal that the apparent physical integrity of polyurethane **1** can be recovered within 2 h at a temperature of 45 °C. To further examine the recovery of the mechanical properties, polyurethane **1** was assessed after a number of different healing times at 45 °C. The data shown in Figure S16 show that after 15 min the mechanical performance of the healed polyurethane **1** depends strongly on the sample preparation (particularly on the initial contact), and thus significant variation occurred. However, in those samples which did heal successfully, there was almost a full recovery of mechanical properties, and the variation could be minimized with longer healing times: after healing for 2 h, reproducible stress–strain curves were generated, and thus here we just compared the mechanical properties after healing for 2 h with the pristine polyurethane **1**. Mean stress–strain curves are shown in Figure 9, and the corresponding mechanical properties calculated from the individual stress–strain curves (see Figure S16) are shown in Table 1. It should be noted that in these experiments the strain was calculated using digital image correlation on images of the specimen surface.[75] The apparent tensile Young's modulus was calculated from the slope of the stress–strain curve between 0 and 4% strain; linear behavior was observed in this region with an R^2 over 0.99. The pristine polyurethane **1** exhibits an apparent tensile Young's modulus of 7.69 MPa when compared to 7.62 MPa for the healed specimen, correlating to a healing efficiency of 99%. The strength at 20% elongation also recovers fully, 0.89 MPa for pristine compared with 0.88 MPa for the healed material. Although the healed material exhibits a minor decrease of the elongation at break and energy absorbed compared with the pristine sample, examination of the standard deviations of all the measurements shows that none of the properties listed in Table 1 change significantly between the pristine and healed materials.

Furthermore, the strain field during tensile tests on the healed polyurethane **1** revealed no significant localization or stress concentration around the healed area; a typical example is shown in Figure 10. In all cases (five specimens) failure occurred elsewhere in the specimen. This data suggests that not only do the global mechanical properties recover during the healing process but also there is no evidence that healing changes the local properties of the polymer in the cut region. Furthermore, during these tests, only one of the five specimens tested was observed to fail in close proximity to the healed region. Together these results suggest excellent recovery of the mechanical properties. The healing temperature of 45 °C is about 10 °C lower than the nominal transition from an elastic behavior to a viscous state (ca. 55 °C in the rheological data): the mobility of the polymer chains is enough to achieve local flow, while maintaining the overall integrity of the specimen shape.

When preparing the healing specimens, the quality of contact between the interfaces (which were neither overlapped nor pressed together, just placed in contact) affects the healing process: good contact facilitates good healing. Hence, there is some advantage if the specimen is able to recover its initial dimensions after deformation. To determine the recovery of the specimen after deformation, creep recovery experiments were performed using the rheometer as well as tests of large strain recovery after tensile loading.

From the rheometer data in Figure 11, it is observed that at 20 °C polyurethane **1** shows good long-term elastic recovery, over 50% deformation can be recovered during the investigating time frame, and creep behavior also shows linear dependence on the stress level, which is attributed to the noncovalent interaction between polymer chains. However, this elastic recovery is very sensitive to temperature, and at 40 °C the elastic recovery is minor. As expected from the earlier rheological data, the temperature dependence of the creep is far from linear: there is a sharp jump from 30 to 40 °C as a result of the disruption of the hydrogen bonding and $\pi-\pi$ stacking interactions. In addition to these experiments tensile tests were performed to characterize the recovery of a large deformation at a faster rate (see Figure 12). Here it is observed that a tensile deformation of 26% recovered by 99% after the release of the loading within 5 min.

CONCLUSION

A well-defined polyurethane **1** capable of self-assembling via aromatic $\pi-\pi$ stacking interactions and hydrogen bonds to generate a healable supramolecular elastomer has been synthesized. Healing of damage to the bulk material can be effected by exposure to a moderate temperature (45 °C) in order to recover both the physical and mechanical characteristics. Analysis of the rheometric shift factor (a_T) normalized to T_g reveals that this polyurethane does not exhibit traditional thermoplastic characteristics but instead shows enhanced ability to flow and an additional relaxation with the disruption of the noncovalent network structures. The dynamics of the healing process was monitored carefully on both a micro- and macroscale, revealing that after 15 min at a temperature of 45 °C a damaged interface can be healed completely. Finally, the recovery of the mechanical properties, characterized by modulus, strength, and energy absorbed before failure, after healing was investigated, and results reveal a full recovery of all these properties with a healing efficiency of ca. 99%, indicating the ability of the polymer network structure to reconstruct at the cut interface, at an easily accessible temperature. Finally, a preliminary experiment indicates that the material is able to

Downloaded by UNIV OF READING on September 8, 2015 | http://pubs.acs.org
Publication Date (Web): August 21, 2015 | doi: 10.1021/acs.macromol.5b01162

DOI: 10.1021/acs.macromol.5b01162
Macromolecules 2015, 48, 6132–6141

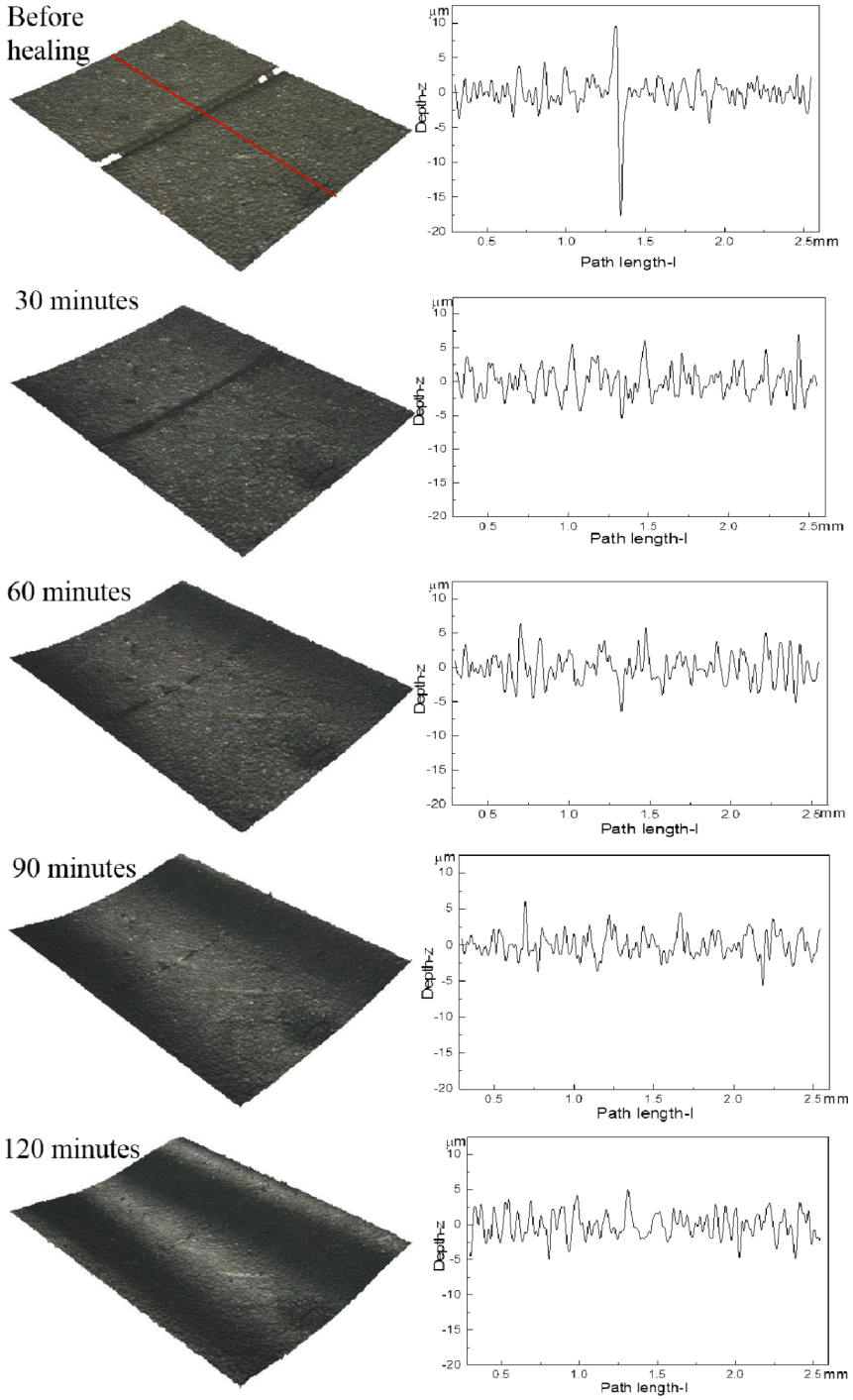

Figure 8. 3D depth profiles of the optical image with the surface profile measurement of the healing process for polyurethane **1** at the temperature of 45 °C every 30 min. The roughness profile is recorded from the middle of the whole sample across the crack horizontally as indicated by the red line in the figure.

recover an applied strain of 25% within 5 min of unloading. The healing and shape recovery properties of this supramolecular polyurethane at an easily accessible temperature will be explored for its applicability in coating and composite formulations with potential in biomedical fields.

EXPERIMENTAL SECTION

Materials. All chemicals and solvents were purchased from Sigma-Aldrich and used as received. Krasol HLBH-P2000 was supplied by Cray Valley.

Characterization. ^{1}H NMR and ^{13}C NMR spectra were recorded on either a Bruker Nanobay 400 or a Bruker DPX 400 spectrometer operating at 400 MHz for ^{1}H NMR or 100 MHz for ^{13}C NMR, respectively. The samples for NMR spectroscopic analysis were prepared in $CDCl_3$ (50 mg/mL), and dissolution was aided with slight heating. The data were processed using MestReNova Version 7.0.2-8636. Chemical shifts (δ) are reported in ppm relative to tetramethylsilane (δ 0.00 ppm) for ^{1}H NMR spectra and to chloroform (δ 77.0 ppm) for the ^{13}C NMR assignment; coupling constants (J) are expressed in hertz (Hz). Infrared spectroscopic analysis employed a PerkinElmer 100 FT-IR spectrometer equipped with a diamond ATR sampling attachment, and samples were analyzed

Downloaded by UNIV OF READING on September 8, 2015 | http://pubs.acs.org
Publication Date (Web): August 21, 2015 | doi: 10.1021/acs.macromol.5b01162

DOI: 10.1021/acs.macromol.5b01162
Macromolecules 2015, 48, 6132−6141

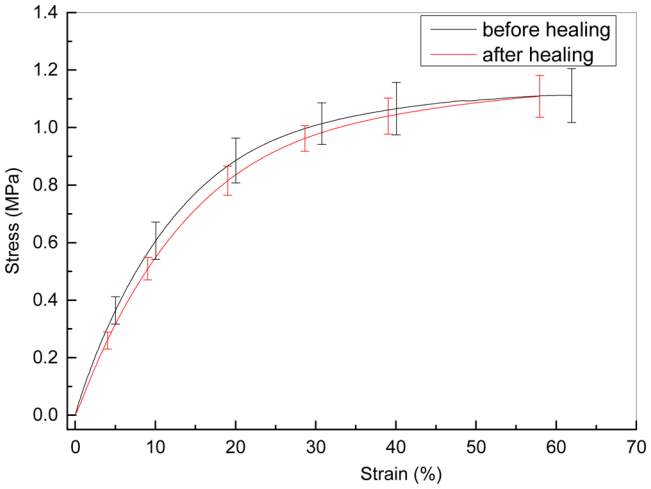

Figure 9. Mean stress−strain curve for pristine and healed polyurethane **1**. The mean values are recorded from five specimens of each material; data from all five specimens are shown in the Supporting Information. Note that in this figure the end of the stress−strain curve does not indicate specimen failure.

Table 1. Mechanical Properties from Tensile Testing for SPU, Means, and (Standard Deviations) from Five Specimens

sample	apparent tensile Young's modulus (MPa)	strength[a] (MPa)	elongation at break (%)	energy absorbed (MJ m^{-3} × 100)
before healing	7.69 (0.52)	0.89 (0.07)	69 (17)	66 (20)
after healing	7.62 (0.45)	0.88 (0.04)	64 (9)	58 (13)

[a]Strength is defined as the stress at 20% strain.

in neat form. The infrared spectroscopic data were processed using Microsoft Excel 2013. Gel permeation chromatography (GPC) was conducted using an Agilent Technologies 1260 Infinity, and the data were processed using Agilent GPC/SEC software; polystyrene was used as the calibrant. Samples for GPC analysis were dissolved in analytical grade THF (2 mg/mL). Differential scanning calorimetric analysis used a TA Instruments DSC 2920, and a three-cycle process was carried out on the solid sample: heating from ambient to +100 °C at a ramp rate of 10 °C min^{-1}, followed by cooling from +100 °C to −70 °C at a ramp rate of −20 °C min^{-1} and then finally by heating from −70 °C to +200 °C at a ramp rate of +20 °C min^{-1}. The sample size used was 8−15 mg, and the data were processed using TA Universal Analysis Version 4.7A. Thermogravimetric analysis employed a TGA Q50 instrument by heating the solid samples (sample size ca. 20 mg) from ambient temperature to +300 °C at a ramp rate of +10 °C min^{-1}. The data were processed using TA Universal Analysis Version 4.7A. SAXS/WAXS was performed using a Bruker Nanostar system. The SAXS data were recorded on a Vantec detector, and the WAXS data were recorded using a FujiFilm image plate system. Samples were mounted in a temperature-controlled heater, in the form of films sandwiched between Kapton films. The SAXS camera length was 66 cm, the q = 2*pi*sin(theta)/lambda (scattering angle = 2*theta, lambda = 1.54 Å) scale was calibrated using silver behenate, and the d-spacing is 58.3 Å. The WAXS IP is a Fujifilm imaging plate (BAS-IP MS 2025), which is read on a Fujifilm FLA-7000 and wiped clean on a Fujifilm IP Eraser 3. The sample to IP distance is 55 mm. The calibrant for WAXS is corundum, which has a d-spacing of 2.55 Å. Single crystal X-ray intensity data were collected on Agilent Gemini S Ultra dual Cu and Mo radiation source, Cu radiation at 1.54 Å, Mo at 0.71 Å, CCD sapphire detector. Data collection was carried out at 150 K.

Sample Preparation for Rheological and Mechanical Assessment. Thin films of the polyurethane were produced for mechanical testing via a solution casting procedure. All of the polyurethanes were dissolved in THF, and the solution was poured into flat PTFE molds. This was subsequently placed in a vacuum oven at 70 °C with a pressure of approximately 0.6−0.8 bar for a duration of 24 h. Polyurethane film of uniform thickness between 200 and 500 μm was obtained at the end of this procedure without residual solvent. Rheometric analysis was performed on circular samples (25 mm diameter) that were obtained from the molded film using a steel punch cutter. For tensile testing, rectangular samples were cut with a razor blade, and paper end-tabs were bonded to the samples with a commercial cyanoacrylate adhesive Loctite. This sample assembly was found to reduce slippage inside the tensile grips of the tensometer. The gauge section between the grips was of 25 mm length, 5 mm width, and approximately 0.5 mm thickness.

Mechanical Testing. Parallel plate oscillatory shear was performed with an Anton Paar Physica MCR 301 rheometer. For the temperature sweep at a single frequency of 5 Hz, the samples were placed on the rheometer, heated to 70 °C, and held at this temperature for approximately 5 min. The samples were then subjected to a cooling temperature ramp of 2 °C/min to 0 °C before being heated up to 120 °C and held at this temperature for 1 h. After this step they were cooled again from 120 to 0 °C at 2 °C/min. During all of these steps the dynamic shear moduli (G', G'', and tan δ) of the samples were

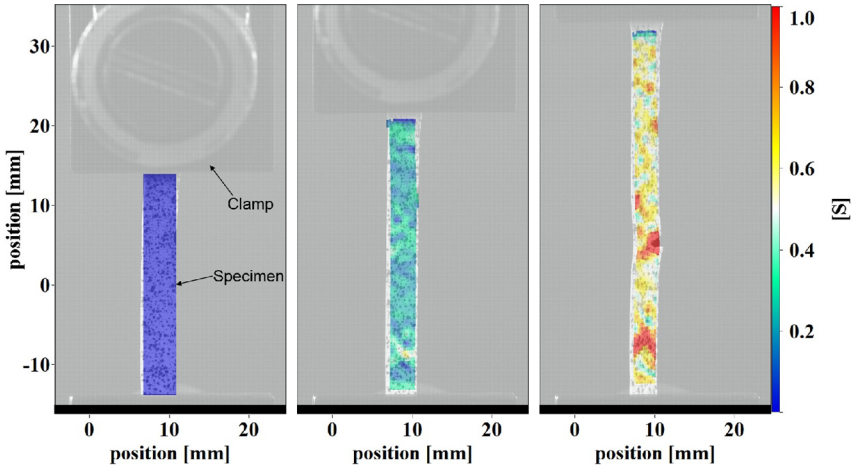

Figure 10. Strain field for healed polyurethane **1** during the tensile test: from left to right corresponding to the initial stage, the middle, and before failure of the tensile test specimen, respectively.

Downloaded by UNIV OF READING on September 8, 2015 | http://pubs.acs.org
Publication Date (Web): August 21, 2015 | doi: 10.1021/acs.macromol.5b01162

DOI: 10.1021/acs.macromol.5b01162
Macromolecules 2015, 48, 6132−6141

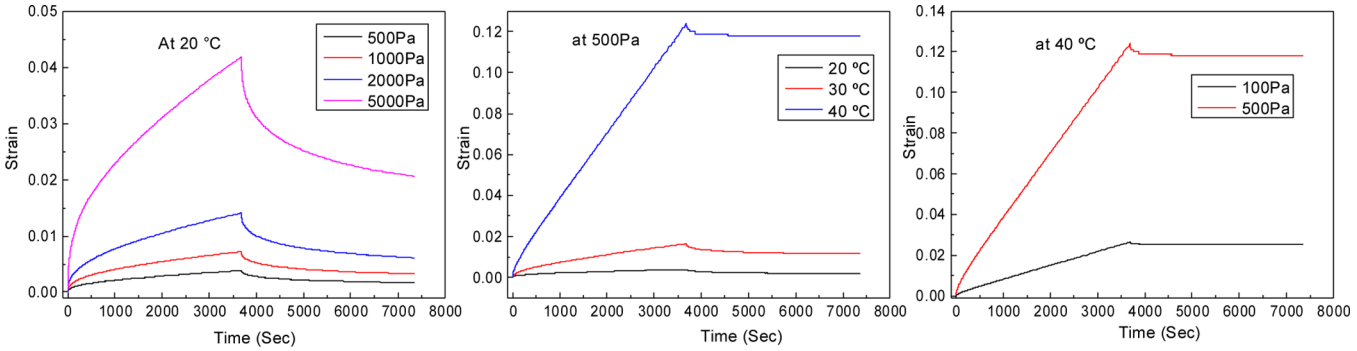

Figure 11. Creep-recovery behavior of polyurethane **1**: (a) stress dependence at 20 °C, (b) temperature dependence at the stress of 500 Pa, and (c) stress dependence at 40 °C.

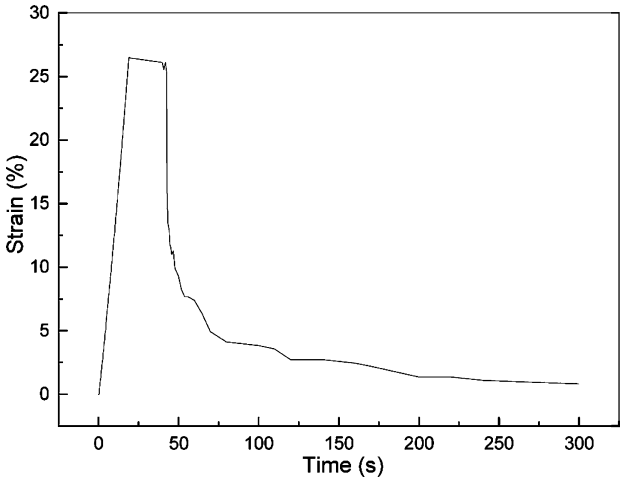

Figure 12. Recovery of the large deformation for polyurethane **1** under tension.

recorded. This method was applied to ensure that chemical cross-linking had not occurred from the exposure of the samples to high temperatures. Cross-linking was not observed during rheological testing; i.e., an increase in G' during the isothermal step at 120 °C was not observed. The samples were tested at a strain amplitude of 0.1%.

For the isothermal frequency sweeps, the samples were again placed in the rheometer and heated to 70 °C for approximately 5 min. The temperature was reduced to 20 °C and again held for 5 min. The frequency sweeps were then performed between 0.1 and 100 rad/s at a strain amplitude of 0.1% for each selected temperature; each time the temperature was held for 5 min before data were gathered. Three cycles of tests were measured, and the results show that the repeating heating does not change the properties significantly (see Figure S13). Creep tests were also carried out at different temperatures and stress levels.

The tensile testing was carried out on an Instron universal testing machine (model 5982) with a 100 N load cell. A constant true strain rate of 0.04 s^{-1} was used, for purposes of controlling the experiment (but not subsequent data analysis) this calculated from the cross-head displacement. At least five samples were tested for each material type. In order to obtain accurate, and full-field displacement and strain data, the digital image correlation technique was used. The surface of the sample was painted with both white and black sprays in order to create a random speckle pattern. During each test, a digital camera (Point Gray GS3-U3-41C6C-C with a Micro-NIKKOR 105 mm lens) was used to record images of the specimen surface at a rate of 5 pictures per second. Approximately a hundred images were thus created before specimen failure. The obtained images were analyzed by commercially available image correlation software (DaVis StrainMaster Software 7.2) to extract displacement and strain maps on the specimen surface. The mean strain was combined with force data from the Instron testing machine to generate stress−strain curves. Furthermore, the strain fields were used to examine the possibility of strain localization around the healed region: none was observed.

For the deformation recovery test, the sample (with speckle pattern) was first loaded to the target strain at the rate of 0.04 s^{-1} by the Instron machine, and then the load was released immediately. The images of the sample during both the loading and unloading were recorded, and the deformation was calculated accordingly.

Polyurethane Synthesis. Methylene diphenyl diisocyanate (11 mmol, 2.75 g) was added to Krasol HLBH-P2000 (5.2 mmol, 11.00 g), and the mixture was stirred for 3 h at 80 °C under a nitrogen atmosphere after which dry THF (80 mL) was added. The reaction was left to cool to room temperature, 4-methoxybenzyl-1-(4-nitrophenyl)methanamine (11.2 mmol, 3.11 g) was then added, and the mixture was stirred for 1 h at 50 °C. THF was then removed *in vacuo*, and the product was purified by multiple slow precipitation in methanol and dried *in vacuo*. The product was isolated as a light orange colored solid (14.42 g, 88%). IR (neat): 2960, 2918, 2862, 2851, 1703, 1604, 1594, 1514, 1459, 1414, 1377, 1342, 1304, 1262, 1220, 1173, 1107. ^{1}H NMR (δ; 400 MHz; $CDCl_3$): 0.83−1.98 (340H, m), 3.80 (6H, s), 3.84 (4H, $_{apt}t$, $_{obs}J$ = 10.5), 4.14−4.16 (4H, m), 4.45 (4H, s), 4.70 (4H, s), 6.47 (2H, br), 6.64 (2H, br), 6.87−7.44 (32H, m), 8.15 (4H, *d*, J = 7.2). ^{13}C NMR (δ; 100 MHz; $CDCl_3$): 10.9, 25.9, 26.8, 29.8, 30.2, 30.7, 33.2, 33.4, 36.1, 38.9, 40.5, 50.4, 55.3, 63.8, 65.3, 114.5, 118.8, 120.5, 123.9, 128.0, 128.3, 129.2, 129.3, 129.4, 129.4, 136.1, 136.4, 136.7, 145.6, 147.2, 153.8, 156.0, 159.4. GPC (THF): M_w 12 121, M_n 6056, and $Đ$ 2.00.

CCDC 1036523 contains the supplementary crystallographic data for urea **2**. These data can be obtained free of charge from The Cambridge Crystallographic Data Centre via www.ccdc.cam.ac.uk/data_request/cif.

■ ASSOCIATED CONTENT

Supporting Information

The Supporting Information is available free of charge on the ACS Publications website at DOI: 10.1021/acs.macromol.5b01162.

Figures S1−S16 and Table S1 (PDF)

■ AUTHOR INFORMATION

Corresponding Author

*Fax (+ 44) 118-378-6331; e-mail w.c.hayes@reading.ac.uk (W.H.).

Notes

The authors declare no competing financial interest.

■ ACKNOWLEDGMENTS

The authors thank EPSRC for funding (EP/J010715/1 and EP/J011436/1) for postdoctoral fellowships for AF, IG and

Downloaded by UNIV OF READING on September 8, 2015 | http://pubs.acs.org
Publication Date (Web): August 21, 2015 | doi: 10.1021/acs.macromol.5b01162

DOI: 10.1021/acs.macromol.5b01162
Macromolecules 2015, 48, 6132−6141

XT) and EP/L020599/1. We are grateful to the University of Reading for access to instrumentation in the Chemical Analysis Facility, to Mr. Nick Spencer for assistance with SAXS/WAXS and Cray Valley for the supply of Krasol HLBH-P2000. C.R.S. and X.T. thank Richard Duffin, Richard Froud, Neil Warland, and Igor Dyson for technical support at Oxford University.

REFERENCES

(1) Engels, H.-W.; Pirkl, H.-G.; Albers, R.; Albach, R. W.; Krause, J.; Hoffmann, A.; Casselmann, H.; Dormish, J. *Angew. Chem., Int. Ed.* **2013**, *52*, 9422−9441.
(2) Shelke, N. B.; Nagarale, R. K.; Kumbar, S. G. In *Natural and Synthetic Biomedical Polymers*; Deng, S. G. K. T. L., Ed.; Elsevier: Oxford, 2014; pp 123−144.
(3) Rivero, G.; Nguyen, L.-T. T.; Hillewaere, X. K. D.; Du Prez, F. E. *Macromolecules* **2014**, *47*, 2010−2018.
(4) Hearon, K.; Gall, K.; Ware, T.; Maitland, D. J.; Bearinger, J. P.; Wilson, T. S. *J. Appl. Polym. Sci.* **2011**, *121*, 144−153.
(5) Zhang, C.; Madbouly, S. A.; Kessler, M. R. *ACS Appl. Mater. Interfaces* **2015**, *7*, 1226−1233.
(6) Eschweiler, N.; Keul, H.; Millaruelo, M.; Weberskirch, R.; Moeller, M. *Polym. Int.* **2014**, *63*, 114−126.
(7) Poljanšek, I.; Fabjan, E.; Moderc, D.; Kukanja, D. *Int. J. Adhes. Adhes.* **2014**, *51*, 87−94.
(8) Woodward, P.; Merino, D. H.; Hamley, I. W.; Slark, A. T.; Hayes, W. *Aust. J. Chem.* **2009**, *62*, 790−793.
(9) Woodward, P. J.; Merino, D. H.; Greenland, B. W.; Hamley, I. W.; Light, Z.; Slark, A. T.; Hayes, W. *Macromolecules* **2010**, *43*, 2512−2517.
(10) Gooch, A.; Murphy, N. S.; Thomson, N. H.; Wilson, A. J. *Macromolecules* **2013**, *46*, 9634−9641.
(11) Klinedinst, D. B.; Yilgör, I.; Yilgör, E.; Zhang, M.; Wilkes, G. L. *Polymer* **2012**, *53*, 5358−5366.
(12) Prisacariu, C.; Scortanu, E.; Stoica, I.; Agapie, B.; Barboiu, V. *Polym. J.* **2011**, *43*, 613−620.
(13) Brunsveld, L.; Folmer, B. J. B.; Meijer, E. W.; Sijbesma, R. P. *Chem. Rev.* **2001**, *101*, 4071−4097.
(14) Bosman, A. W.; Sijbesma, R. P.; Meijer, E. W. *Mater. Today* **2004**, *7*, 34−39.
(15) Merino, D. H.; Slark, A. T.; Colquhoun, H. M.; Hayes, W.; Hamley, I. W. *Polym. Chem.* **2010**, *1*, 1263−1271.
(16) Gooch, A.; Nedolisa, C.; Houton, K. A.; Lindsay, C. I.; Saiani, A.; Wilson, A. J. *Macromolecules* **2012**, *45*, 4723−4729.
(17) Doehler, D.; Michael, P.; Binder, W. In *Self-Healing Polymers: From Principles To Applications*; Binder, W. H., Ed.; Wiley-VCH: Weinheim, 2013; pp 7−60.
(18) Greenland, B. W.; Fiore, G. L.; Rowan, S. J.; Weder, C. In *Healable Polymer Systems*; The Royal Society of Chemistry: London, 2013; pp 92−125.
(19) Bergman, S. D.; Wudl, F. *J. Mater. Chem.* **2008**, *18*, 41−62.
(20) White, S. R.; Sottos, N. R.; Geubelle, P. H.; Moore, J. S.; Kessler, M. R.; Sriram, S. R.; Brown, E. N.; Viswanathan, S. *Nature* **2001**, *409*, 794−797.
(21) Blaiszik, B. J.; Caruso, M. M.; McIlroy, D. A.; Moore, J. S.; White, S. R.; Sottos, N. R. *Polymer* **2009**, *50*, 990−997.
(22) Cordier, P.; Tournilhac, F.; Soulie-Ziakovic, C.; Leibler, L. *Nature* **2008**, *451*, 977−980.
(23) Burattini, S.; Greenland, B. W.; Chappell, D.; Colquhoun, H. M.; Hayes, W. *Chem. Soc. Rev.* **2010**, *39*, 1973−1985.
(24) Chen, Y.; Guan, Z. *Chem. Commun.* **2014**, *50*, 10868−10870.
(25) Burattini, S.; Colquhoun, H. M.; Fox, J. D.; Friedmann, D.; Greenland, B. W.; Harris, P. J. F.; Hayes, W.; Mackay, M. E.; Rowan, S. J. *Chem. Commun.* **2009**, 6717−6719.
(26) Coulibaly, S.; Roulin, A.; Balog, S.; Biyani, M. V.; Foster, E. J.; Rowan, S. J.; Fiore, G. L.; Weder, C. *Macromolecules* **2014**, *47*, 152−160.
(27) Zhang, H.; Han, D.; Yan, Q.; Fortin, D.; Xia, H.; Zhao, Y. *J. Mater. Chem. A* **2014**, *2*, 13373−13379.
(28) Wang, Z.; Urban, M. W. *Polym. Chem.* **2013**, *4*, 4897−4901.
(29) Chen, Y.; Kushner, A. M.; Williams, G. A.; Guan, Z. *Nat. Chem.* **2012**, *4*, 467−472.
(30) Montarnal, D.; Tournilhac, F.; Hidalgo, M.; Couturier, J.-L.; Leibler, L. *J. Am. Chem. Soc.* **2009**, *131*, 7966−7967.
(31) Ghosh, B.; Urban, M. W. *Science* **2009**, *323*, 1458−1460.
(32) Lu, Y.-X.; Guan, Z. *J. Am. Chem. Soc.* **2012**, *134*, 14226−14231.
(33) Rowan, S. J.; Cantrill, S. J.; Cousins, G. R. L.; Sanders, J. K. M.; Stoddart, J. F. *Angew. Chem., Int. Ed.* **2002**, *41*, 898−952.
(34) Corbett, P. T.; Leclaire, J.; Vial, L.; West, K. R.; Wietor, J.-L.; Sanders, J. K. M.; Otto, S. *Chem. Rev.* **2006**, *106*, 3652−3711.
(35) Peterson, A. M.; Jensen, R. E.; Palmese, G. R. *ACS Appl. Mater. Interfaces* **2010**, *2*, 1141−1149.
(36) Montarnal, D.; Capelot, M.; Tournilhac, F.; Leibler, L. *Science* **2011**, *334*, 965−968.
(37) Capelot, M.; Montarnal, D.; Tournilhac, F.; Leibler, L. *J. Am. Chem. Soc.* **2012**, *134*, 7664−7667.
(38) Cho, S. H.; Andersson, H. M.; White, S. R.; Sottos, N. R.; Braun, P. V. *Adv. Mater.* **2006**, *18*, 997−1000.
(39) Toohey, K. S.; Sottos, N. R.; Lewis, J. A.; Moore, J. S.; White, S. R. *Nat. Mater.* **2007**, *6*, 581−585.
(40) Caruso, M. M.; Blaiszik, B. J.; White, S. R.; Sottos, N. R.; Moore, J. S. *Adv. Funct. Mater.* **2008**, *18*, 1898−1904.
(41) Burattini, S.; Greenland, B. W.; Merino, D. H.; Weng, W.; Seppala, J.; Colquhoun, H. M.; Hayes, W.; Mackay, M. E.; Hamley, I. W.; Rowan, S. J. *J. Am. Chem. Soc.* **2010**, *132*, 12051−12058.
(42) Greenland, B. W.; Burattini, S.; Hayes, W.; Colquhoun, H. M. *Tetrahedron* **2008**, *64*, 8346−8354.
(43) Burattini, S.; Colquhoun, H. M.; Greenland, B. W.; Hayes, W. *Faraday Discuss.* **2009**, *143*, 251−264.
(44) Burattini, S.; Greenland, B. W.; Hayes, W.; Mackay, M. E.; Rowan, S. J.; Colquhoun, H. M. *Chem. Mater.* **2011**, *23*, 6−8.
(45) Fox, J.; Wie, J. J.; Greenland, B. W.; Burattini, S.; Hayes, W.; Colquhoun, H. M.; Mackay, M. E.; Rowan, S. J. *J. Am. Chem. Soc.* **2012**, *134*, 5362−5368.
(46) Vaiyapuri, R.; Greenland, B. W.; Colquhoun, H. M.; Elliott, J. M.; Hayes, W. *Polym. Chem.* **2013**, *4*, 4902−4909.
(47) Gale, P. A.; Sessler, J. L.; Steed, J. W. *Chem. Commun.* **2011**, *47*, 5931−5932.
(48) Fiore, G. L.; Rowan, S. J.; Weder, C. *Chem. Soc. Rev.* **2013**, *42*, 7278−7288.
(49) Du, P.; Wu, M.; Liu, X.; Zheng, Z.; Wang, X.; Sun, P.; Joncheray, T.; Zhang, Y. *New J. Chem.* **2014**, *38*, 770−776.
(50) Hart, L. R.; Harries, J. L.; Greenland, B. W.; Colquhoun, H. M.; Hayes, W. *Polym. Chem.* **2013**, *4*, 4860−4870.
(51) Chen, S.; Yuan, H.; Zhuo, H.; Chen, S.; Yang, H.; Ge, Z.; Liu, J. *J. Mater. Chem. C* **2014**, *2*, 4203−4212.
(52) Rekondo, A.; Martin, R.; de Luzuriaga, A.; Cabanero, G.; Grande, H. J.; Odriozola, I. *Mater. Horiz.* **2014**, *1*, 237−240.
(53) Yoon, J. A.; Kamada, J.; Koynov, K.; Mohin, J.; Nicolay, R.; Zhang, Y.; Balazs, A. C.; Kowalewski, T.; Matyjaszewski, K. *Macromolecules* **2012**, *45*, 142−149.
(54) Canadell, J.; Goossens, H.; Klumperman, B. *Macromolecules* **2011**, *44*, 2536−2541.
(55) Mauldin, T. C.; Kessler, M. R. *Int. Mater. Rev.* **2010**, *55*, 317−346.
(56) Guimard, N. K.; Oehlenschlaeger, K. K.; Zhou, J.; Hilf, S.; Schmidt, F. G.; Barner-Kowollik, C. *Macromol. Chem. Phys.* **2012**, *213*, 131−143.
(57) Van Gemert, G. M. L.; Peeters, J. W.; Söntjens, S. H. M.; Janssen, H. M.; Bosman, A. W. *Macromol. Chem. Phys.* **2012**, *213*, 234−242.
(58) Oya, N.; Ikezaki, T.; Yoshie, N. *Polym. J.* **2013**, *45*, 955−961.
(59) Agnaou, R.; Capelot, M.; Tencé-Girault, S.; Tournilhac, F.; Leibler, L. *J. Am. Chem. Soc.* **2014**, *136*, 11268−11271.
(60) Burnworth, M.; Tang, L.; Kumpfer, J. R.; Duncan, A. J.; Beyer, F. L.; Fiore, G. L.; Rowan, S. J.; Weder, C. *Nature* **2011**, *472*, 334−337.

Downloaded by UNIV OF READING on September 8, 2015 | http://pubs.acs.org
Publication Date (Web): August 21, 2015 | doi: 10.1021/acs.macromol.5b01162

DOI: 10.1021/acs.macromol.5b01162
Macromolecules 2015, 48, 6132−6141

(61) Bode, S.; Zedler, L.; Schacher, F. H.; Dietzek, B.; Schmitt, M.; Popp, J.; Hager, M. D.; Schubert, U. S. *Adv. Mater.* **2013**, *25*, 1634−1638.
(62) Bode, S.; Bose, R. K.; Matthes, S.; Ehrhardt, M.; Seifert, A.; Schacher, F. H.; Paulus, R. M.; Stumpf, S.; Sandmann, B.; Vitz, J.; Winter, A.; Hoeppener, S.; Garcia, S. J.; Spange, S.; van der Zwaag, S.; Hager, M. D.; Schubert, U. S. *Polym. Chem.* **2013**, *4*, 4966−4973.
(63) Hart, L. R.; Hunter, J. H.; Nguyen, N. A.; Harries, J. L.; Greenland, B. W.; Mackay, M. E.; Colquhoun, H. M.; Hayes, W. *Polym. Chem.* **2014**, *5*, 3680−3688.
(64) Ahmed, B.; Yusuf, M. *Indian J. Chem. Sect. B: Org. Chem. Incl. Med. Chem.* **2010**, *49*, 241−246.
(65) Modak, A.; Dutta, U.; Kancherla, R.; Maity, S.; Bhadra, M.; Mobin, S. M.; Maiti, D. *Org. Lett.* **2014**, *16*, 2602−2605.
(66) Clemitson, I. *Castable Polyurethane Elastomers*; Taylor & Francis Group: New York, 2008.
(67) Kaushiva, B. D.; Wilkes, G. L. *J. Appl. Polym. Sci.* **2000**, *77*, 202−216.
(68) Ferry, J. D. *Viscoelastic Properties of Polymers*; Wiley: New York, 1980.
(69) Onogi, S.; Masuda, T.; Kitagawa, K. *Macromolecules* **1970**, *3*, 109−116.
(70) Stadler, F. J.; Pyckhout-Hintzen, W.; Schumers, J.-M.; Fustin, C.-A.; Gohy, J.-F.; Bailly, C. *Macromolecules* **2009**, *42*, 6181−6192.
(71) Liu, C.-Y.; He, J.; Keunings, R.; Bailly, C. *Macromolecules* **2006**, *39*, 8867−8869.
(72) Liu, C.-Y.; Halasa, A. F.; Keunings, R.; Bailly, C. *Macromolecules* **2006**, *39*, 7415−7424.
(73) Wei, Q.; Wang, J.; Shen, X.; Zhang, X. A.; Sun, J. Z.; Qin, A.; Tang, B. Z. *Sci. Rep.* **2013**, *3*, 1093.
(74) Taskin, O. S.; Kiskan, B.; Yagci, Y. *Macromolecules* **2013**, *46*, 8773−8778.
(75) Schreier, H.; Orteu, J.-J.; Sutton, M. A. *Image Correlation for Shape, Motion and Deformation Measurements*; Springer: Boston, MA, 2009.

Downloaded by UNIV OF READING on September 8, 2015 | http://pubs.acs.org
Publication Date (Web): August 21, 2015 | doi: 10.1021/acs.macromol.5b01162

DOI: 10.1021/acs.macromol.5b01162
Macromolecules 2015, 48, 6132−6141